12-20-2002

Characteristics of Quasi-Monochromatic Gravity Waves Observed with Na Lidar in the Mesopause Region at Starfire Optical Range, NM

Xiong Hu

Alan Z. Liu
Embry Riddle Aeronautical University - Daytona Beach, liuz2@erau.edu

Chester S. Gardner

Gary R. Swenson

Characteristics of quasi-monochromatic gravity waves observed with Na lidar in the mesopause region at Starfire Optical Range, NM

Xiong Hu

Wuhan Institute of Physics and Mathematics, The Chinese Academy of Sciences, Wuhan, China

Alan Z. Liu, Chester S. Gardner, and Gary R. Swenson

Department of Electrical and Computer Engineering, University of Illinois at Urbana-Champaign, Illinois, USA

Received 22 February 2002; revised 22 May 2002; accepted 2 July 2002; published 20 December 2002.

[1] The University of Illinois Na wind/temperature lidar data collected at the Starfire Optical Range, NM, between Jan. 1998 and May 2000 was used to extract the dominant monochromatic gravity waves. By using simultaneously measured horizontal wind and temperature profiles, the vertical wavelengths (λ_z), (T_I), and propagation directions were determined using the hodograph method. A total of 700 monochromatic gravity waves were analyzed from ~300 h of observations. It was found that 84.4% of the waves were propagating upwards. The mean λ_z was 12.6 km and 9.9 km for upward and downward propagating waves, respectively, and showed a bimodal distribution with the largest number of waves at 15–17 km and 7–9 km. The mean T_I is ~10 h. There is no dominant direction of propagation. For waves with λ_z <11 km, the percentage of upward propagating waves is lower (71%). *INDEX TERMS:* 3334 Meteorology and Atmospheric Dynamics: Middle atmosphere dynamics (0341, 0342); 3360 Remote sensing; 3384 Waves and tides. **Citation:** Hu, X., A. Z. Liu, C. S. Gardner, and G. R. Swenson, Characteristics of quasi-monochromatic gravity waves observed with Na lidar in the mesopause region at Starfire Optical Range, NM, *Geophys. Res. Lett.*, *29*(24), 2169, doi:10.1029/2002GL014975, 2002.

1. Introduction

[2] Atmospheric gravity waves (GWs) play a major role in the dynamics of the atmosphere in the mesopause region. Observations and statistics of data are needed to characterize the GWs' spectral, temporal, and spatial variations. Quasi-monochromatic (QM) GWs are frequently observed with airglow imagers, lidars and radars. The QM waves observed with imagers typically have short horizontal wavelength (λ_h) and high frequency [*Hecht et al.*, 2001; *Walterscheid et al.*, 1999], while those observed by radars and lidars typically have long λ_h and low frequency [*Gavrilov et al.*, 1996].

[3] Hodograph method has been widely used to analyze QM waves observed by radar and lidar. *Gavrilov et al.* [1996] used this method with MU radar 3-D wind data and showed that there were relatively more waves with larger λ_z. *Namboothiri et al.* [1996] used both MU radar horizontal wind and lidar Na density data and obtained GW's propagation directions. The λ_z of QM waves can be related to the intrinsic frequency through GW's dispersion relations [*Gardner and Voelz*, 1986]. *Swenson et al.* [1995] showed that GW's with large λ_z can penetrate to higher altitudes.

0094-8276/02/2002GL014975$05.00

[4] The University of Illinois Na Wind/Temperature lidar at the Starfire Optical Range (SOR, 35°N, 106.5°W), NM, provides simultaneous measurements of 3-D wind, temperature and Na density profiles with high temporal and vertical resolutions, which allows GWs to be directly characterized. *Yang* [1998] applied the hodograph method in the data collected in 1994 and 1995 at SOR to characterize QM waves. In this study, the Na wind/temperature lidar data accumulated at SOR from 1998 to 2000 were used to characterize the intrinsic parameters of QM waves with hodograph method.

2. Data Analysis

2.1. Data

[5] There are a total of 45 nights or 300 h of wind and temperature data acquired between Jan. 1998 and May 2000. The data between 84 km and 104 km were used. The original data was smoothed to 1 km in the vertical direction and temporally averaged every 30 min. Therefore, only the waves with $2 < \lambda_z < 20$ km and period between 1 h and 20 h were considered.

2.2. Hodograph Method

[6] A wave propagating in $x-z$ plane can be expressed as,

$$(u', v', T') = e^{z/2H}\Re\left[(\hat{u}, \hat{v}, \hat{T})e^{i(kx+mz-\omega t)}\right], \quad (1)$$

where u' is the in-phase wind along the wave propagation direction, v' is the quadrature-phase wind perpendicular to the wave propagation direction, T' is the temperature perturbation, k and m are horizontal and vertical wavenumbers, respectively, and ω is the frequency. The GW polarization relations are

$$\hat{v} = -i(f/\omega)\hat{u}, \quad (2)$$

$$\hat{T} = H[im + 1/(2H)](\omega^2 - f^2)/(\omega kR)\hat{u}, \quad (3)$$

where H is the scale height, R is the gas constant and f is the inertial frequency. In the Northern Hemisphere where $f > 0$, (2) shows that $\hat{v}$ will lead $\hat{u}$ for upward propagating waves, i.e. the (u', v') vector will rotate clockwise with increasing altitude. Similarly, according to (3), for upward propagating waves ($m < 0$), $\hat{T}$ will lead $\hat{u}$ for waves propagating in positive x direction, and the (u', T') vector will rotate clockwise with increasing altitude. These rotations are reversed for waves propagating in the opposite direction. This information can be used to determine both the horizontal and vertical propagation directions.

[7] The intrinsic frequency can be calculated by the amplitude ratio between $\hat{u}$ and $\hat{v}$ based on (2). The background shear perpendicular to the wave's horizontal propagation direction can affect this estimation [*Hines*, 1989]. To minimize this effect, we defined a factor $D = |(1/N)\,(dV/dz)/(f/\omega)|$, where N is the buoyancy frequency. For waves with $D > 0.3$, the wind shear effect was considered significant and they were excluded in the analysis.

2.3. Gravity Wave Model

[8] The QM waves are modeled as [*Yang*, 1998],

$$U'_m = Ue^{\beta(z-z_0)}\cos[m(z-z_0)+\theta_u], \tag{4}$$

$$V'_m = Ve^{\beta(z-z_0)}\cos[m(z-z_0)+\theta_v], \tag{5}$$

$$T'_m = Te^{\beta(z-z_0)}\cos[m(z-z_0)+\theta_T], \tag{6}$$

where β is the growth factor, $z_0 = 94$ km, U'_m, V'_m and T'_m are perturbations of zonal and meridional wind and temperature with vertical wavenumber m, respectively.

[9] The amplitudes of the wind component along the major and minor axes of the polarization ellipse, $|\hat{u}|$ and $|\hat{v}|$, and the azimuth φ of the major axis can be calculated by using the following formula [*Gavrilov et al.*, 1996],

$$\varphi = \frac{1}{2}\left(\pi n + \arctan\frac{2F_{uv}}{V^2-U^2}\right), \tag{7}$$

$$2|\hat{u}|^2 = U^2 + V^2 + \left[\left(V^2-U^2\right)^2 + 4F_{uv}^2\right]^{1/2}, \tag{8}$$

$$2|\hat{v}|^2 = U^2 + V^2 - \left[\left(V^2-U^2\right)^2 + 4F_{uv}^2\right]^{1/2}, \tag{9}$$

where $F_{uv} = UV\cos(\theta_u - \theta_v)$. The integer $n = 1$ when $V < U$. When $V > U$, $n = 0$ and 2 for $F_{uv} > 0$ and $F_{uv} < 0$, respectively, in order for $0 \leqslant \varphi \leqslant \pi$.

2.4. Analysis Technique

[10] The procedure of the analysis is to first determine the λ_z of the dominant wave from the perturbation power spectrum, then fit the perturbation according to GW model to derive other intrinsic parameters. The first step is to derive the wind and temperature perturbations. Linear fits on each nightly mean wind profiles were used as the background winds. A fourth order polynomial fit on each nightly mean temperature profile was used as the background temperature. The perturbation profiles were obtained by subtracting the backgrounds from the original profiles. A linear trend in altitude of each profile was then removed to minimize the contamination of tidal oscillations and long λ_z waves.

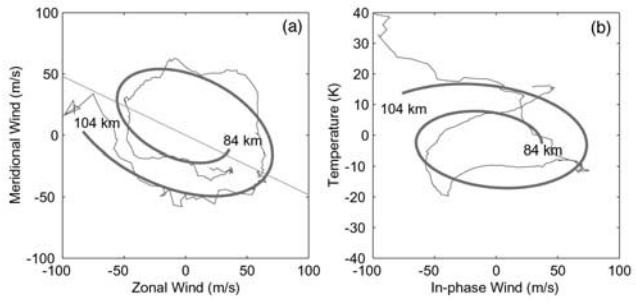

Figure 1. Hodographs of (a) the zonal wind versus meridional wind and (b) the in-phase wind versus temperature at 3:30 UT on Sep. 8, 1999. The thin lines are measured data. The thick lines are the fitted spiral. The azimuth angle of the wave propagation direction is 115.7°+ 180° = 295.7°. It is indicated by a straight line in (a).

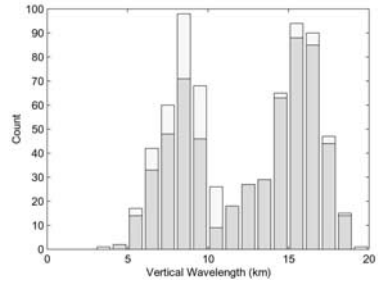

Figure 2. Histogram of the vertical wavelengths of all 700 extracted waves. Darker (lighter) shading indicates upward (downward) propagating waves.

[11] The λ_z of the dominant wave was determined by finding the peak in the mean power spectrum of the zonal wind, meridional wind and the scaled temperature for each set of perturbation profiles. The temperature perturbation was scaled to make it comparable to and in the same unit with the wind perturbation, by multiplying it with $g/(T_0N_0)$, where g is the gravity acceleration, T_0 and N_0 are the nightly mean temperature and buoyancy frequency, respectively. The spectral resolution was enhanced by padding the perturbation profiles with zeros prior to computing their spectra. A λ_z was accepted when its corresponding peak power was above the 95% confidence level and an empirically determined threshold. The threshold was used to make sure only waves with significant amplitudes were extracted.

[12] After the λ_z was determined, the wave parameters were deduced by fitting the GW model (4)–(6) to both wind and temperature perturbation profiles. The major axis angle φ was then calculated, and the horizontal coordinates were rotated so that the x-axis was along the major axis. This fitting was then repeated in the new coordinates and a new φ was obtained. When φ converged to within 0.1°, the iteration was stopped and the first dominant wave was extracted. This wave was then subtracted from the perturbation profiles and the above process was repeated to find the next dominant wave. On average, 2 to 5 waves can be reliably extracted from each profile [*Yang*, 1998]. Waves extracted after the 2nd wave usually had very small amplitude. In this study, we only considered the 1st and 2nd waves.

3. Results and Discussions

3.1. An Example Case

[13] Figure 1a shows the hodograph for zonal and meridional winds and their wave fits. This inertial GW with λ_z of 14.7 km was observed at 3:30 UT on Aug. 12, 1999. The

Table 1. Mean Values of Intrinsic Period τ, Vertical and Horizontal Wavelengths (λ_z and λ_h) of Extracted QM Waves for All Waves and for Waves With $\lambda_z < 11$ km

	up	down	all
τ (all λ_z) (h)	10.5	8.5	10.2
τ ($\lambda_z < 11$ km) (h)	10.3	8.7	9.8
λ_z (all λ_z) (km)	12.6	9.9	12.2
λ_z ($\lambda_z < 11$ km) (km)	8.0	8.6	8.2
λ_h (all λ_z) (10^3 km)	2.25	1.32	2.11
λ_h ($\lambda_z < 11$ km) (10^3 km)	1.42	1.19	1.36

hodograph is a spiral, not an ellipse, because of the exponential increase of amplitude with altitude. The rotation is clockwise, indicating an upward propagating wave. From the fitted spiral, we can determine that the direction of its major axis is 115.7° or 115.7° + 180° (The direction is defined to be 0° at north and increases clockwise). If we choose the 115.7° direction, then the hodograph of the (u', T') (Figure 1b) shows a counter-clockwise spiral. This indicates that horizontal wave propagation direction is opposite to the 115.7° direction, i.e. is towards $\varphi = 115.7° + 180° = 295.7°$.

3.2. Distribution of λ_z, λ_h and Intrinsic Period

[14] There are a total of 700 QM waves obtained as the 1st or 2nd wave from 45 nights of data. Of all the waves, 591 waves (84.4%) propagated upwards and 109 (15.6%) downwards. The mean values of wave parameters are listed in Table 1. The mean λ_z are 12.6 km and 9.9 km for the upward and downward waves, respectively. The histogram of λ_z for upward and downward waves is shown in Figure 2. It shows a bimodal distribution with the largest number of waves at about 15–17 km and 7–9 km.

[15] Figure 3 shows the histograms of λ_z separately for the 1st and 2nd waves. Most of the 1st waves have λ_z of 15–17 km, while most of the 2nd waves have λ_z of 7–9 km. These two waves are not harmonically related, however, since we found no correlation in the propagation direction nor the period between the 1st and the 2nd waves extracted from the same profiles.

[16] The histogram of λ_h (Figure 4a) does not show a bimodal distribution. The largest number of waves have λ_h between 500 and 2000 km. There is no dominant direction of propagation (Figure 4b), although there is a slight preference toward the northeast and southwest. The intrinsic period (Figure 5a) has a bell shaped distribution, with the peak at around 10–11 h.

3.3. Limitation of the 20 km Altitude Range

[17] The 20 km altitude range of the data may limit the accuracy of the extracted long wavelength waves ($\lambda_z > 10$ km). This is due to the possible contamination by waves with $\lambda_z > 20$ km and $<\sim 40$ km. These waves cannot be extracted with the 20 km data range but their effect cannot be fully removed by detrending. Such waves include the semidiurnal tide (SDT), which has a λ_z between 20–40 km in winter [*Franke and Thorsen*, 1993]. The influence of the SDT in the summer is expected to be small because of its much longer λ_z (>100 km). In winter, the SDT may contaminate the 15–17 km QM waves we obtained.

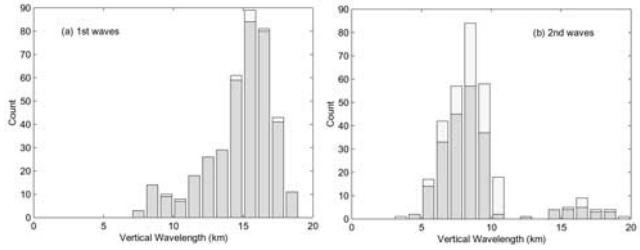

Figure 3. Same as Figure 2 except are shown separately for the 1st (a) and the 2nd (b) extracted waves.

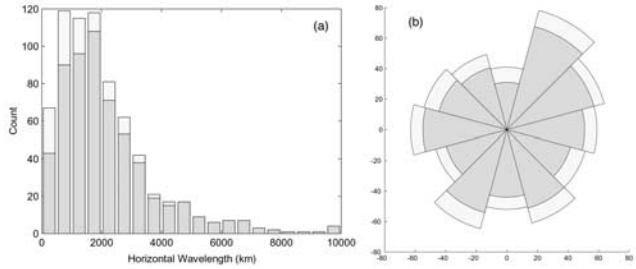

Figure 4. Histograms of (a) horizontal wavelengths (b) and propagation direction. North is up and east is right. Darker (lighter) shading indicates upward (downward) propagating waves.

[18] To address this issue, we performed Monte-Carlo simulations to examine the effect of SDT on the extracted waves. We used the Jan. SDT data from the Global Scale Wave Model (GSWM) [*Hagan et al.*, 1999], which has a temperature amplitude of 5–15 K from 85 to 100 km. This amplitude is comparable to or larger than observations [*Palo et al.*, 1997; *States and Gardner*, 2000]. We found that it was not large enough to produce erroneous waves with our algorithm because its power spectrum didn't exceed our threshold (about 60% too low). This indicates that under nominal conditions, the SDT does not have strong influence to the extracted QM waves. Nevertheless, the SDT amplitude in the real atmosphere can be much stronger in any individual night. Therefore some of the extracted waves with λ_z between 15–17 km may be contaminated. In addition, the presence of SDT also increased the uncertainty of extracted intrinsic period.

[19] Our simulation also showed that the presence of SDT did not have noticeable effect on short λ_z waves. We therefore separately plotted histograms for waves with $\lambda_z < 11$ km only, i.e. waves that were not contaminated. Their mean parameters are also listed in Table 1. There are 223 (71%) waves propagating upward and 91 (29%) waves downward. Com-

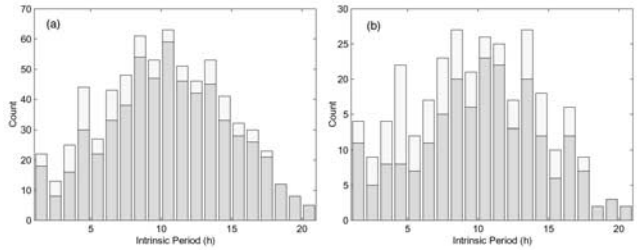

Figure 5. (a) Histograms of intrinsic periods for (a) all 700 extracted waves and (b) waves with $\lambda_z < 11$ km. Darker (lighter) shading indicates upward (downward) propagating waves.

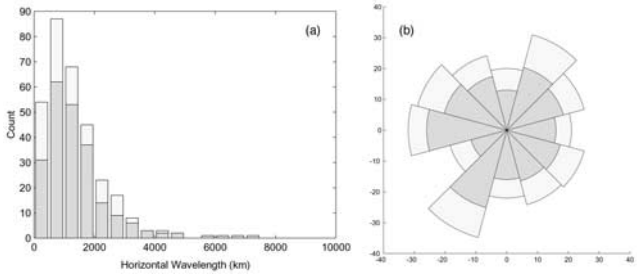

Figure 6. Same as Figure 4 but only includes waves with $\lambda_z < 11$ km.

pared with the distribution of all waves, the intrinsic period (Figure 5b) shows a similar bell shaped distribution. The horizontal wavelength (Figure 6a) has a narrower distribution with a smaller mean value. The propagation direction (Figure 6b) also shows similar distribution, with north-east and south-west being the most frequent directions.

4. Summary

[20] A total of 300 h of Na wind/temperature data were used to characterize the quasi-monochromatic inertial gravity waves with the hodograph method. A total of 700 waves were obtained. The majority of them (84.4%) propagated upwards. The percentage is similar to that obtained by *Lintelman and Gardner* [1994], who computed the unambiguous vertical wavenumber spectra to determine the fraction of energy propagating upward and downward based on 350 hours of Na lidar data at Urbana, Illinois.

[21] The λ_z showed a bimodal distribution with the most frequently observed waves having λ_z of about 15–17 km and 7–9 km. We have verified that the 15–17 km and 7–9 km waves are not harmonically related. The possible contamination to the 15–17 km waves by waves with $\lambda_z > 20$, such as SDT is minimized by removing the linear trend in altitude. Monte-Carlo simulations with GSWM data suggest that this contamination is not likely a significant source to the extracted 15–17 km wave.

[22] The distribution of amplitudes versus vertical wavelengths and the distribution of intrinsic phase speed versus in-phase wind fall within the linear instability limit (not shown). The waves with relatively large λ_z usually have relatively large amplitudes. They can be more frequently observed than those with relatively small λ_z. The bimodal distribution of λ_z is very intriguing. Most of the 1st extracted waves, i.e. the dominant waves, have λ_z of 15–17 km. There is very little waves in the 12–14 km range. It may be related to the wave source and filtering through the middle atmosphere.

[23] **Acknowledgments.** Dr. Hu likes to thank the Chinese Academy of Sciences for supporting his visit to the University of Illinois, and appreciate Prof. Xunxie Zhang's support. Comments from two reviewers and Editor Dr. Miyahara greatly improved the manuscript and are very much appreciated. The lidar data acquisition and analysis are supported by NSF Aeronomy program through grant ATM 97-09921. We are indebted to the USAF and specifically Dr. Robert Fugate and the Air Force personnel for their support in field operations. Some support was also extended from studies of high frequency waves through NSF grant ATM 97-14620.

References

Franke, S. J., and D. Thorsen, Mean winds and tides in the upper middle atmosphere at Urbana (40N, 88W) during 1991–1992, *J. Geophys. Res.*, *98*, 18,607–18,615, 1993.

Gardner, C. S., and D. G. Voelz, Lidar studies of the nighttime sodium layer over Urbana, Illinois, 1, Seasonal and nocturnal variations, *J. Geophys. Res.*, *91*, 3659–3673, 1986.

Gavrilov, N. M., S. Fukao, T. Nakamura, T. Tsuda, M. D. Yamanaka, and M. Yamamoto, Statistical analysis of gravity waves observed with the middle and upper atmosphere radar in the middle atmosphere 1, Method and general characteristics, *J. Geophys. Res.*, *101*, 29,511–29,521, 1996.

Hagan, M. E., M. D. Burrage, J. M. Forbes, J. Hackney, W. J. Randel, and X. Zhang, GSWM-98: Results for migrating solar tides, *J. Geophys. Res.*, *104*, 6813–6827, 1999.

Hecht, J. H., R. L. Walterscheid, M. P. Hickey, and S. J. Franke, Climatology and modeling of quasi-monochromatic atmospheric gravity waves observed over Urbana Illinois, *J. Geophys. Res.*, *106*, 5181–5195, 2001.

Hines, C. O., Tropopausal mountain waves over Arecibo - A case study, *J. Atmos. Sci.*, *46*, 476–488, 1989.

Lintelman, S. A., and C. S. Gardner, Observation and interpretation of the spectra of atmospheric gravity wave perturbations with upward and downward phase progression, *J. Geophys. Res.*, *99*, 16,959–16,972, 1994.

Namboothiri, S. P., T. Tsuda, M. Tsutsumi, T. Nakamura, C. Nagasawa, and M. Abo, Simultaneous observations of mesospheric gravity waves with the MU radar and a sodium lidar, *J. Geophys. Res.*, *101*, 4057–4063, 1996.

Palo, S. E., et al., An intercomparison between the GSWM, UARS, and ground based radar observations: A case-study in January 1993, *Ann. Geophys.*, *15*, 1123–1141, 1997.

States, R. J., and C. S. Gardner, Thermal structure of the mesopause region (80–105 km) at 40°N latitude. Part II: Diurnal variations, *J. Atmos. Sci.*, *57*, 78–92, 2000.

Swenson, G. R., C. S. Gardner, and M. J. Taylor, Maximum altitude penetration of atmospheric gravity waves observed during ALOHA-93, *Geophys. Res. Lett.*, *22*, 2857–2860, 1995.

Walterscheid, R. L., J. H. Hecht, R. A. Vincent, I. M. Reid, J. Woithe, and M. P. Hickey, Analysis and interpretation of airglow and radar observations of quasi-monochromatic gravity waves in the upper mesosphere and lower thermosphere over Adelaide, Australia (35°S, 138°E), *J. Atmos. Sol.-Terr. Phys.*, *61*, 461–478, 1999.

Yang, W. M., Gravity wave studies of the mesopause region using a Na wind/temperature lidar, Ph.D. Thesis, University of Illinois, 1998.

X. Hu, Wuhan Institute of Physics and Mathematics, The Chinese Academy of Sciences, P.O. Box 71010, Wuhan 430071, China. (xhu@wipm.ac.cn)

A. Z. Liu, C. S. Gardner, and G. R. Swenson, Department of Electrical and Computer Engineering, University of Illinois at Urbana-Champaign, 1308 West Main St., Urbana, IL 61801, USA. (liuzr@uiuc.edu; cgardner@uillinois.edu; swenson1@uiuc.edu)